

MAGNETARS VS. HIGH MAGNETIC FIELD PULSARS: A THEORETICAL INTERPRETATION OF THE APPARENT DICHOTOMY

JOSE A. PONS¹ AND ROSALBA PERNA²

Draft version November 19, 2018

ABSTRACT

Highly magnetized neutron stars (NSs) are characterized by a bewildering range of astrophysical manifestations. Here, building on our simulations of the evolution of magnetic stresses in the NS crust and its ensuing fractures (Perna & Pons 2011), we explore in detail, for the middle-age and old NSs, the dependence of star-quake frequency and energetics on the relative strength of the poloidal (B_p) and toroidal (B_{tor}) components. We find that, for $B_p \gtrsim 10^{14}$ G, since a strong crustal toroidal field $B_{\text{tor}} \sim B_p$ is quickly formed on a Hall timescale, the initial toroidal field needs to be $B_{\text{tor}} \gg B_p$ to have a clear influence on the outbursting behaviour. For initial fields $B_p \lesssim 10^{14}$ G, it is very unlikely that a middle-age ($t \sim 10^5$ years) NS shows any bursting activity. This study allows us to solve the apparent puzzle of how NSs with similar dipolar magnetic fields can behave in a remarkably different way: an outbursting ‘magnetar’ with a high X-ray luminosity, or a quiet, low-luminosity, ‘high- B ’ radio pulsar. As an example, we consider the specific cases of the magnetar 1E 2259+586 and the radio pulsar PSR J1814-1744, which at present have a similar dipolar field $\sim 6 \times 10^{13}$ G. We determine for each object an initial magnetic field configuration that reproduces the observed timing parameters at their current age. The same two configurations also account for the differences in quiescent X-ray luminosity and for the ‘magnetar/outbursting’ behaviour of 1E 2259+586 but not of PSR J1814-1744. We further use the theoretically predicted surface temperature distribution to compute the light-curve for these objects. In the case of 1E 2259+586, for which data are available, our predicted temperature distribution gives rise to a pulse profile whose double-peaked nature and modulation level is consistent with the observations.

Subject headings: stars: magnetars — stars: neutron — X-rays: bursts

1. INTRODUCTION

Neutron stars, end points of the evolution of massive stars, are characterized by a bewildering variety of astrophysical manifestations. Among these, particularly intriguing is a class of slow rotators ($P \sim 2 - 11$ sec) with an especially high quiescent X-ray luminosity ($L_x \sim 10^{33} - 10^{35}$ erg), almost always exceeding their rotational energy loss \dot{E} , and displaying occasional energetic outbursts and giant flares. The latter can release energies as large as $\sim 10^{45}$ erg.

The source of energy responsible for powering the outbursts and flares, and enhancing the quiescent emission, is believed to be of magnetic origin (Thompson & Duncan 1995, 2001). The magnetic field evolves in the NS interior under the effects of Ohmic dissipation, Hall drift and Ambipolar diffusion, although this latter has recently been suggested to play a lesser role in the presence of superfluid matter (Glampedakis, Jones & Samuelsson 2011). In this case, the evolution of the magnetic field causing the magnetar activity would likely take place in the stellar crust. However, if the observational evidence from the cooling of the supernova remnant in Cassiopeia A (Page et al. 2011; Shternin et al. 2011) is confirmed, it would imply that the object is undergoing a core superfluid transition at 5×10^8 K. In the magnetar context, higher core temperatures are expected and the transition to core superfluidity can be significantly delayed, as originally suggested by Arras, Cumming & Thompson (2004). Therefore, the role of ambipolar diffusion in the core remains an open question. In this work we focus on the role of Ohmic diffusion and Hall drift in the crust.

Occasionally the magnetic stress exceeds locally the tensile strength of the crust, causing it to fracture; the ensuing sudden release of elastic and magnetic energy powers the outbursts. This picture, in which the magnetic field strength ‘regulates’ the properties of an object, i.e. its appearance as an outbursting magnetar, or a ‘normal’, quiet radio pulsar, left many unanswered questions and unsolved puzzles. Why some objects are more active than others? What determines the frequency and energetics of events? Why some objects have been observed to emit very energetic γ -ray flares (the so-called ‘Soft Gamma-ray Repeater’, (SGRs)), while others only display less energetic X-ray bursts (the so-called ‘Anomalous X-ray Pulsars’ (AXPs))? Is there a real difference between these two classes? And, if the magnetic field is the main driving force, how is it possible for a ‘low B ’-field pulsar to undergo an outburst (Rea et al. 2010)? Altogether, how can two objects, characterized by an almost identical magnetic field (as inferred through measurements of the pulsar period P and its derivative \dot{P}) manifest themselves as apparently different objects with respect to those properties which should be driven by the B -field strength (outbursting behaviour, quiescent X-ray luminosity)? This apparent dichotomy is exemplified by the magnetar 1E 2259+586, with an inferred dipolar field of 5.9×10^{13} G, and the ‘high- B ’ field radio pulsar PSR J1814-1744, with an inferred $B_{\text{dip}} = 5.5 \times 10^{13}$ G. The former is classified as an AXP; it was observed to have an active period of outbursts in 2002 (Woods et al. 2004), and has an enhanced X-ray luminosity in quiescence, $L_x \sim 10^{34}$ erg, which exceeds its rotational energy loss. On the other hand, PSR J1814-1744 appears to be a ‘normal’, quiet radio pulsar (Camilo et al. 2000), with no discernible X-ray emission in the X-ray band.

In order to understand from first principles what is the phys-

¹ Department de Física Aplicada, Universitat d’Alacant, Ap. Correus 99, 03080, Alacant, Spain

² JILA and Department of Astrophysical and Planetary Science, University of Colorado at Boulder, 440 UCB, Boulder, CO, 80304

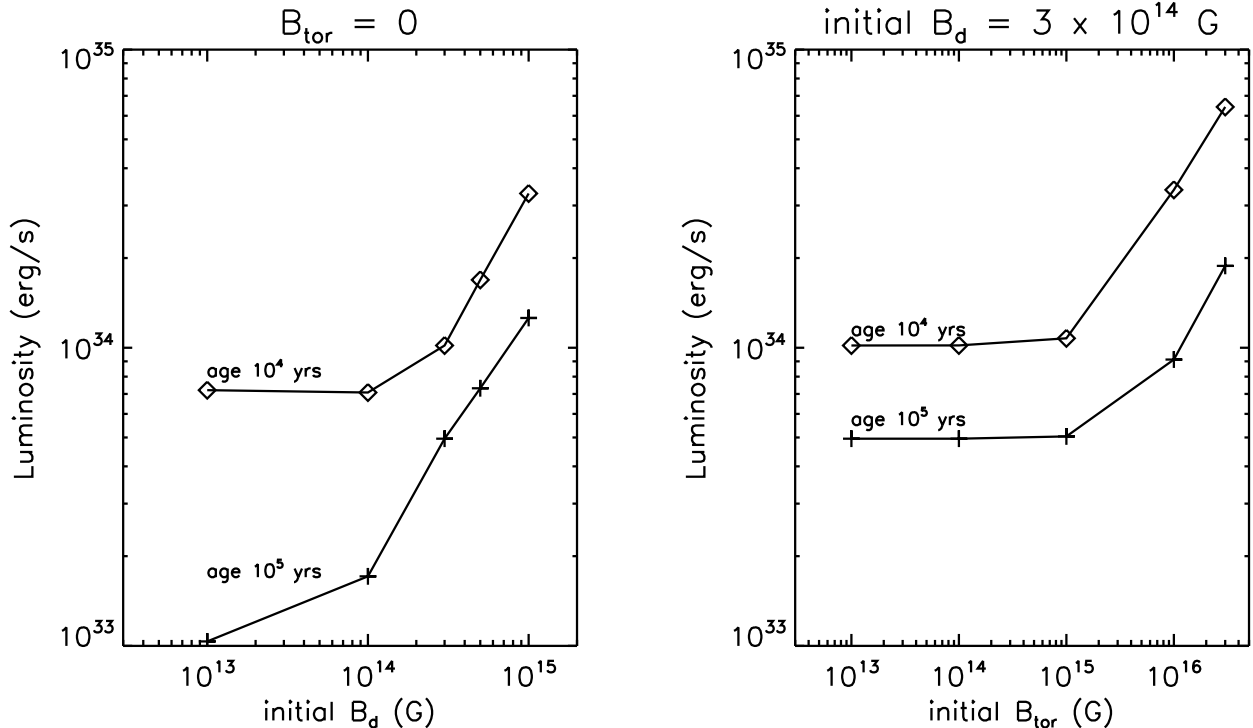


FIG. 1.— Luminosity at two different ages as a function of the initial magnetic field. Left panel: dependence of the luminosity on the initial poloidal field (at pole) for models with $B_{\text{tor}} = 0$. Right panel: same for models with $B_p = 3 \times 10^{14}$ G and different strength of the initial toroidal field.

ical origin of the variety of observed phenomenology, in Perna & Pons (2011; PP2011 in the following), we performed the first long-term 2D simulations that followed the evolution of magnetic stresses in the NS crust; these, combined with calculations of the breaking stress of the NS, allowed us to theoretically predict frequency, energetics, and location on the NS surface of the outbursts (associated with crust fractures). Our results allowed us to establish that there is no fundamental difference among apparently different manifestations of the objects (such as ‘AXPs’ and ‘SGRs’). We also found that both the dipolar component and the ‘hidden’ toroidal component play an equally important role in determining the frequency and energetics of the starquakes. Furthermore, for a given initial B -field configuration and strength, younger objects yield more frequent and more energetic outbursts.

In this follow up paper, we continue our work in several respects. Firstly, we extend our study of the outburst frequency and energetics to focus on the influence of the relative strengths of the poloidal and toroidal field components. This study allows us to uncover some fundamental clues as to what creates the varied phenomenology of the highly magnetized neutron star family. Second, for the middle-aged and older objects, we consider the mutual influence of the magnetic and thermal evolution and predict, for a combination of B_p and B_{tor} initial strengths, the X-ray luminosity, temperature, timing properties and magnetic field at current age. Last, as an example, we consider two specific objects, 1E 2259+586 and PSR J1814-1744, which, as described above, have almost identical spin parameters and hence inferred dipolar B field, but very different manifestations. For each of them, we show how we can find an initial B -field configuration that reproduces their observed timing parameters at their current timing age, as well as account for the differences in quiescent X-ray luminosity, and for the ‘magnetar/outbursting’ behaviour of 1E 2259+586 but not PSR J1814-1744. We also compute

the surface temperature distributions associated with the magnetic configurations that reproduce those properties and use them to compute the expected X-ray light-curves in quiescence. For the case of 1E 2259+586, for which data are available, we show that the qualitative features that we predict are a good match to the data.

The paper is organized as follows. The magneto-thermal evolution is described in §2, together with predictions for the intensity of the X-ray luminosity with age as a function of B_p and B_{tor} . In §3, we study the dependence of the starquake frequency and energetics on the relative strengths of B_p and B_{tor} . The specific examples of magneto-thermal evolution for 1E 2259+586 and PSR J1814-1744 are presented in §4. We summarize and discuss our work in §5.

2. MAGNETO-THERMAL EVOLUTION OF HIGHLY MAGNETIZED NEUTRON STARS

The first attempt to study the long term cooling of magnetized NSs, including all realistic microphysics and taking into account magnetic field decay was made by Aguilera et al. (2008). They assumed a simple, analytical law for the time variation of B_p which incorporates the main features of the Ohmic and Hall terms in the induction equation. Numerical simulations of the magnetic field evolution in a realistic neutron star crust, including the nonlinear effects of the Hall term were presented in Pons & Geppert (2007), but in this case assuming an isothermal crust. The fully coupled magneto-thermal evolution of a NS was later studied by Pons, Miralles & Geppert (2009). However, owing to numerical difficulties in treating the Hall term, their models could include only Ohmic diffusion. A fully coupled evolutionary simulation has not been possible up to now, but for initial values of $B_p \lesssim 10^{15}$ G, the effect of the Hall drift is expected to introduce at most quantitative changes (a somewhat faster dissipation) with respect to the purely Ohmic pic-

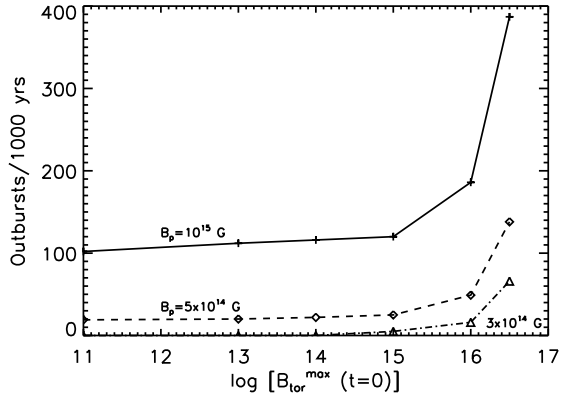


FIG. 2.— Average number of outbursts per 1000 years as a function of the initial toroidal field strength, for a 10^5 years old neutron star. We show results for three different initial poloidal fields: $B_p(t=0) = 10^{15}$ G (solid lines), $B_p(t=0) = 5 \times 10^{14}$ G (dashes), and $B_p(t=0) = 3 \times 10^{14}$ G (dash-dotted lines).

ture described in Pons, Miralles & Geppert (2009), which can be considered a good approximation to reality. With this code, we performed a number of simulations of our baseline model (a $1.4M_\odot$ NS with a radius of 11.6 km, and moment of inertia $I = 1.4 \times 10^{45}$ g cm 2) varying the initial values of the dipolar and internal toroidal fields. We refer to Pons, Miralles & Geppert (2009) and Aguilera et al. (2008) for all technical details about the code and the microphysical input. The minimal cooling scenario (Page et al. 2004), without exotic phases nor fast neutrino cooling processes, was assumed. We also include enhanced neutrino emission from the breaking and formation of neutron Cooper pairs in the core, consistently with the observational evidence from the cooling of the supernova remnant in Cassiopeia A (Page et al. 2011; Shternin et al. 2011).

As noted in previous studies, the average luminosity of a NS born with $B_p < 5 \times 10^{13}$ G, is hardly affected, compared to the non-magnetized case. On the other hand, those NSs born as magnetars are subject to significant heating by the dissipation of currents in the crust. At fixed poloidal field, the luminosity of models with strong internal toroidal components is systematically higher than that of models without toroidal fields, due to the additional energy reservoir stored in the toroidal field, which is gradually released as the field dissipates. In Fig. 1 we show the dependence of the luminosity at a fixed age as a function of the initial magnetic field. We can see that, for low initial dipolar fields, the luminosity barely changes with increasing dipolar field but, once we enter in the magnetar range, $B_p > 10^{14}$ G, a further increase in B_p results in a luminosity increase of more than one order of magnitude. At fixed poloidal field, the existence of an internal toroidal field has no evident effect if $B_{\text{tor}} \lesssim B_p$, but the luminosity is again largely increased when the internal toroidal field exceeds B_p . This can be understood with the following back-of-the-envelope estimate. The rate at which magnetic energy e_m is dissipated can be approximated by

$$\frac{de_m}{dt} \approx \frac{J^2 V}{\sigma} \quad (1)$$

where $J = \frac{c}{4\pi} \nabla \times B$ is the current density, V is the volume where currents are dissipated (the crust volume) and σ is the electrical conductivity. Approximating $\nabla \times B \approx B/L$, where L is a typical scale-length, and for typical neutron star condi-

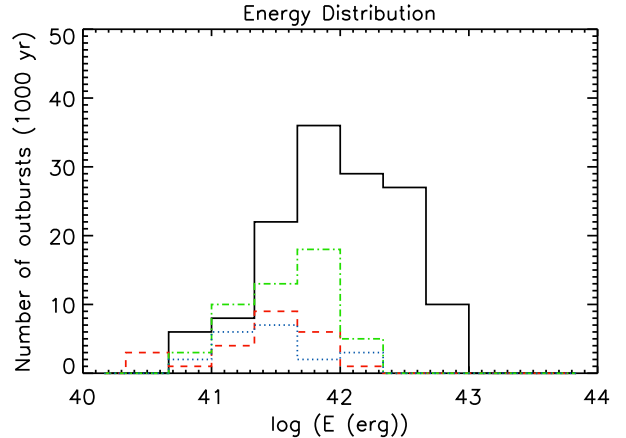


FIG. 3.— Outburst energy distribution of objects at age 10^5 yr born with $B_p = 5 \times 10^{14}$ G and four different initial toroidal fields: $B_{\text{tor}} = 0$ (blue dots), 10^{15} G (red dashes), 10^{16} G (green dash-dotted line), and 3×10^{16} G (black solid line). The total number of outbursts corresponds to a period of 1000 yr.

tions we have, for $L = 1$ km, that

$$\frac{de_m}{dt} \approx 10^{33} \frac{B_{15}^2}{\sigma_{24}} \text{erg/s}. \quad (2)$$

Here B_{15} is the magnetic field in units of 10^{15} G and σ_{24} is the electrical conductivity in units of 10^{24} s $^{-1}$. In order for the internal field to have a significant effect on the luminosity, the dissipation rate of magnetic energy has to be larger than the luminosity in the non-magnetic case. This explains the right panel of Fig. 1, where the influence of the toroidal field only becomes visible after a critical value of 10^{15} G and then increases rapidly with the field strength.

We must remind that the quoted values of B_p and B_{tor} correspond to the initial values. In the models with stronger fields, as a result of the average higher temperatures, the crustal electrical resistivity is also enhanced and magnetic diffusion is more efficient during the first $10^5 - 10^6$ years of a NS's life. As a consequence, all NSs born with fields $\gtrsim 5 \times 10^{14}$ G are subject to faster dissipation. Typically, the dipolar field decreases by a factor of 2-3 in the first 10^5 years of a NS life, and it asymptotically reaches a similar field strength ($\approx 2 - 3 \times 10^{13}$ G) at very late times, irrespectively of the initial strength. The toroidal field at 10^5 years is reduced (on average) by one order of magnitude with respect to the initial value. Note also that, even if the initial model has no toroidal field, for sufficiently large (poloidal fields $\gtrsim 5 \times 10^{14}$ G) the Hall drift will create a toroidal field of similar strength.

3. OUTBURST FREQUENCIES AS A FUNCTION OF THE STRENGTH OF THE DIPOLAR AND TOROIDAL B -FIELD COMPONENTS

In PP2011, we used the numerical code by Pons & Geppert (2007) to follow in axial symmetry the evolution of the magnetic field in the crust of the neutron star. The magnetic stress $M_{ij}(r, \theta, t) = B_i(r, \theta, t)B_j(r, \theta, t)/4\pi$ is computed at each time as a function of the latitude θ on the surface of the star, and the radial coordinate r in the NS crust. As the magnetic field evolves, the crust moves through a series of equilibrium states, during which elastic stresses balance variations in magnetic stresses. If, during the evolution, any component of the magnetic stress departs from its equilibrium value by an amount comparable (or exceeding) the breaking stress of the crust, the crust will break, releasing the accumulated elastic energy (for technical details of the calculations, see PP2011). The simulations allowed PP2011 to predict the frequency and energet-

ics of the starquakes, for a certain initial B -field configuration characterized by a poloidal and a toroidal component. The case of $B_p = 8 \times 10^{14}$ G and $B_{\text{tor}} = 2 \times 10^{15}$ G was considered in detail in that work. It was shown how both the frequency and the energetic of the outbursts decrease with the NS age. Some initial exploration of the role of different initial field strengths further showed that the toroidal component does play a very important role in the outburst properties.

The former study was limited by the numerical restrictions of the code that do not allow to perform a systematic study of the starquake frequency and energetics of objects with $\gtrsim 10^5$ yr with the non-linear terms (too long runs). In order to overcome the numerical difficulties we have adopted a hybrid approach. Since, for these objects, the Hall time is much shorter than their age, we expect that the initial configuration relaxes to a nearly *Hall-neutral* geometry on a few Hall timescales ($t_{\text{Hall}} = 4\pi n_e e L^2 / (cB) \sim 6000 B_{14}^{-1}$ yr), after which the evolution becomes dominated by Ohmic diffusion (Pons & Geppert 2007). Thus, as a first approximation, we follow the NS evolution up to 10^5 yr with the code of Pons, Miralles & Geppert (2009), and then use the temperature and magnetic field profiles as initial input for the short-term, fully non-linear evolution including the Hall term, using the numerical code by Pons & Geppert (2007). The caveat of this approach is that it does not account for possible fast, Hall-induced, initial changes of the magnetic field geometry and strength that may occur for magnetar conditions. This can result in a dissipation of the initial field in, at most, a factor of 2, as estimated in Pons & Geppert (2007). It is also important to note that, whatever the initial geometry of the toroidal field was, it is rapidly (Hall timescale) driven to a similar shape that corresponds to a sort of quasi-steady state. Therefore, our results for middle aged NSs ($\gtrsim 10^5$ yr) are expected to be rather insensitive to the particular form of the toroidal field, being more relevant the role of global quantities (total energy or helicity) that are explored by varying the normalization of the toroidal component.

Our main results concerning the outburst frequency and energetics are summarized in Fig. 2 and Fig. 3. In Fig. 2 we show the dependence of the average number of expected outbursts in a period of 1000 yr on the strength of the initial magnetic field. We have taken the parameter $\epsilon = 0.9$ (see PP2011). We can see that the average outburst rate is sensitive to both B_p and B_{tor} in a similar way as the luminosity. Below a critical poloidal field $B_p < 3 \times 10^{14}$ G the burst rate is vanishingly small ($< 10^{-3}$ yr $^{-1}$), except for very large toroidal fields $B_{\text{tor}} > 10^{16}$ G, but even in that extreme case the outburst frequency is smaller than one per century. For initial $B_p > 3 \times 10^{14}$ G, the outburst rate grows exponentially with the value of B_p . At a fixed B_p , the dependence on the toroidal field is very weak until $B_{\text{tor}} \sim B_p$, but the outburst rate again increases rapidly with increasing values of $B_{\text{tor}} > B_p$. It should be noted that these numbers must be taken with caution, simply as an order of magnitude estimate. The large uncertainties about the internal geometry of the magnetic field and details of the crustal fracture mechanisms do not allow a precise calculation. Nevertheless, these estimates may serve as an indication of the average outburst frequency for objects with similar conditions. The energy distribution of the events during a period spanning 1000 years is shown in Fig. 3, for the model with $B_p = 5 \times 10^{14}$ G and four different toroidal fields. Except for the model with the largest B_{tor} , there is no significant variation in the outburst average

event energy, which is predominantly in the range $10^{41} - 10^{42}$ erg. Only for the extreme case of $B_{\text{tor}} = 3 \times 10^{16}$ G, in addition to the large increase in the number of events, the average outburst energy is also substantially larger, up to 10^{43} erg, reflecting the larger energy reservoir available in the toroidal field.

4. 1E 2259+586 AND PSR J1814-1744: SIMILAR B_p BUT DIFFERENT ASTROPHYSICAL MANIFESTATION

The comprehensive study performed in the previous two sections allows us to obtain a physical explanation to an apparent puzzle in neutron star theory. How can two objects have a very similar dipolar field but display a markedly different behaviour, if the magnetic field provides the main driving force?

Our magnetothermal simulations provide an answer to this question: for a similar inferred value of the dipolar component of the magnetic field, the strength of the internal toroidal field can have a dramatic influence on the behaviour of the neutron star, and in particular on its manifestation as an X-ray bright, outbursting ‘magnetar’, or an X-ray dim, quiet ‘high- B ’ radio pulsar. In the previous section we have shown that, if the *initial* dipolar component is low ($\lesssim \times 10^{14}$ G), the toroidal component, even if strong, is not very effective in producing frequent outbursts. On the other hand, for dipolar field strengths on the order of a few $\times 10^{14}$ G, a toroidal component of the same strength is produced during the evolution, even if it was not there initially. Thus, the importance of an existing initial B_{tor} is only evident when it exceeds the poloidal component. As our results have shown, over ages of about 10^5 yr, a dipolar B -field of a few 10^{14} G roughly halves. It is especially interesting to note that it is around dipolar magnetic fields of $6-7 \times 10^{13}$ G (and ages of about 10^5 yr) that objects classified as ‘magnetars’ or ‘high- B ’ radio pulsars are found to coexist. The most notable examples, as discussed in §1, are 1E 2259+586 and an inferred $B_p = 5.9 \times 10^{13}$ G and magnetar characteristics, and PSR J1814-1744, with $B_p = 5.5 \times 10^{13}$ G and properties of a ‘normal’ radio pulsar. We do not include other interesting objects in this study, such as the high magnetic field radio pulsars PSR J1119-6127 or PSR J1846-0258, because they are very young (≈ 1 kyr) and a fully coupled treatment of the Hall term with the thermal evolution would be required. We have however also examined the high- B radio pulsar PSR J1718-3718, and found that the properties of this object can be well explained by the same model used for PSR J1814-1744, but in an earlier stage. In the remaining of this section we specifically focus on the cases of 1E 2259+586 and PSR J1814-1744 and we leave a more extensive study of many different objects for the future.

We evolved in time our baseline NS varying only the initial B -field configurations (characterized by B_p and B_{tor}) trying to reproduce the timing, the magnetic, and the thermal properties of these two objects at their measured timing age. We assume an orthogonal rotator (angle between the magnetic axis and rotation axis of 90°), and initial spin period of 1 ms, short enough to have no influence on the late-time timing properties. The two models that would represent the two objects under discussion are presented in the following.

1E 2259+586.

This X-ray pulsar is characterized by a period $P = 6.97$ s and period derivative $\dot{P} = 4.8 \times 10^{-13}$ s/s (Gavriil & Kaspi 2002),

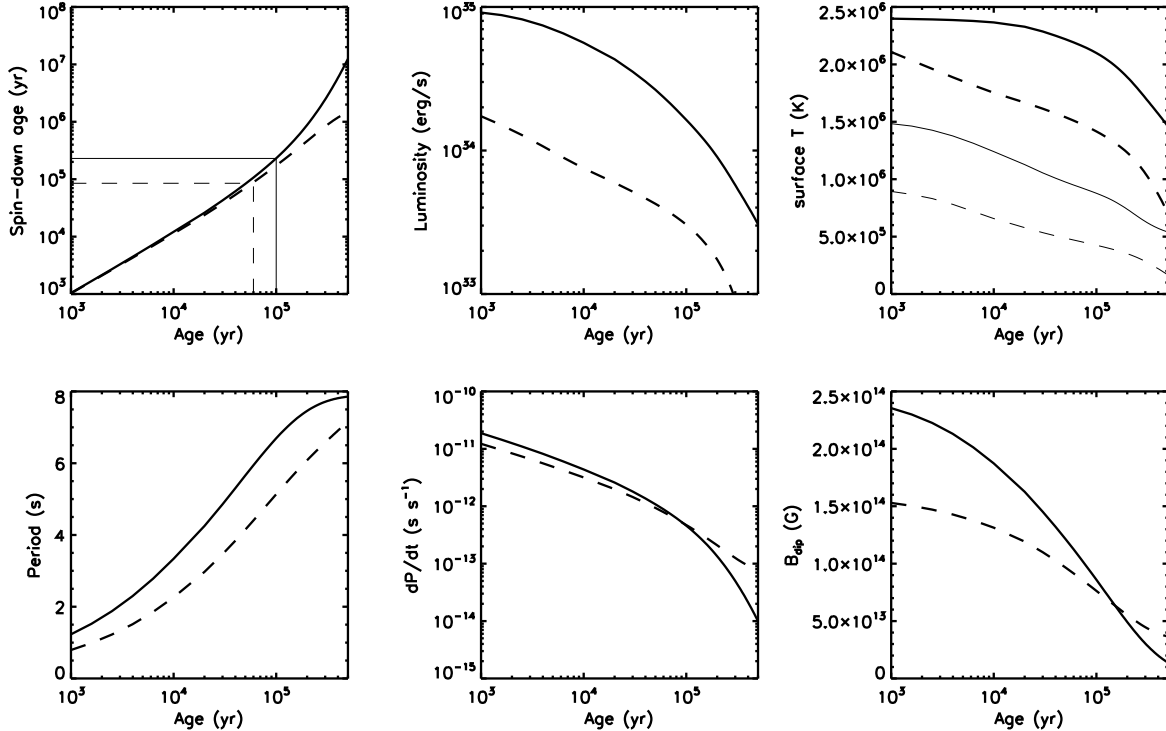


FIG. 4.— Evolution of timing, thermal and magnetic variables for some choices of initial magnetic field configuration that reproduce the observed properties of 1E 2259+586 (solid line) and PSR J1814-1744 (dashed line). The spin-down ages of 230 kyr and 85 kyr are reached at real ages of 100 kyr and 60 kyr, respectively (*top left* panel). In the upper *top right* panel the evolution of the redshifted temperature at the pole (thick) and the equator (thin) is shown for both models.

implying a timing age of $\tau = 230$ kyr. Its X-ray luminosity in the 2-10 keV band of 3.4×10^{34} erg/s (for a distance of 4 kpc, Tian et al. 2010), much larger than its rotational energy, prompted its classification as an AXP. The discovery of a major outburst in 2002 (Kaspi et al. 2003) further tightened the connection between this AXP and the SGRs, and established its 'magnetar-like' nature, despite the low inferred dipolar field of $B_p = 5.9 \times 10^{13}$ G. The quiescent (pre-outburst) spectrum of this object is characterized by the superposition of a thermal and a power-law component. The former, if fitted with a simple blackbody (BB), yields a BB temperature of about 0.4 keV and a BB radius of about 5.3 km. The pulse profile is double peaked (see Woods et al. 2004 for a summary of the pre-outburst spectral properties). The modulation level (or pulsed fraction, PF) was measured in two XMM observations prior to the outburst (Woods et al. 2004); of interest here are the two softest bands (0.3-1.0 and 1.0-2.0 keV), dominated by the thermal component; the measured PF was found to be 0.169 ± 0.015 in the 0.3-1.0 keV band and 0.195 ± 0.006 in the 1-2 keV band in the first of the two observations, and 0.215 ± 0.006 in the 0.3-1.0 keV band and 0.225 ± 0.003 in the 1-2 keV band in the second observation (quoted errors are 1σ ; note that there is some variability between the measured values in the two observations).

Fig. 4 (solid lines) shows an example of such evolution. The initial magnetic field has components $B_p = 2.5 \times 10^{14}$ G and $B_{\text{tor}} = 2.5 \times 10^{16}$ G. In the upper left panel we see how the timing age of the source increasingly departs from the real age. At the measured spin-down age of 230 kyr, the real age of the object is 100 kyr. At this age the predicted luminosity of the object (in its thermal component, computed by integration of the temperature profile over the whole surface of the

star) is about 2×10^{34} erg/s, its period about 6.7 s, its spin-down rate about 4.6×10^{-13} s/s, and its B_p about 6.7×10^{13} G. Note that our realistic NS model described in Section 2 has a different radius and moment of inertia from the canonical values (10 km, 10^{45} g cm²) usually assumed to infer B_p . Our goal is not to make a formal fit to the properties of this object, but simply to show typical examples of representative objects within a class. Nevertheless, the quantities in Fig. 1 are a very close match to the corresponding observed properties of this object. For the thermal quantities (luminosity, temperature), the comparison should however be made with care. The measured luminosity is in fact subject to the uncertainty in distance, and is also model-dependent. Our simulations also predict the temperature profile during the pulsar evolution. We show the evolution of the surface temperature at the pole and the equator in the upper right panel of Fig. 4. A direct comparison between our results and the observations can only be done at a qualitative level at this stage. In fact, while our predictions specifically refer to the thermal luminosity, the measured X-ray luminosity has both a thermal and a non-thermal (powerlaw, PL) component (e.g. Woods et al. 2004). The flux ratio PL/BB is a function of phase, varying between 0.3 and 0.55 in the 0.5-7 keV energy band. If the non-thermal part is due to reprocessing of the thermal photons, then the comparison should be made with the total luminosity, but if the non-thermal photons are of different origin, then only the thermal component should be considered.

In addition, the temperature inferred at infinity depends on both the compactness ratio M/R of the star, and the assumed model atmosphere, which greatly affects the spectrum. For the same NS compactness ratio (and hence same gravitational redshift), fits with Hydrogen atmospheres yield lower effec-

tive temperatures T_{atm} . The exact ratio $T_{\text{BB}}/T_{\text{atm}}$ depends on a number of factors, such as atmosphere composition, magnetic field strength, temperature, and, to a lesser extent, on column density and instrument type (see e.g. Suleimanov et al. 2011 for recent work using non-magnetic model atmospheres with varying composition). An extensive exploration of $T_{\text{BB}}/T_{\text{atm}}$ for different values of the above parameters was made by D. Lloyd with detailed magnetized Hydrogen atmosphere models (Lloyd 2003). For a B -field strength of about 10^{13} G, a surface temperature of $1-2 \times 10^5$ K, and a column density $\sim 10^{21}$ cm $^{-2}$, he found the ratio $T_{\text{BB}}/T_{\text{atm}}$ to be ≈ 2 (using the ACIS-1 spectra simulator). The observed spectrum of 1E 2259+586 has been fitted with a BB+PL before the outburst (Woods et al. 2004), and with both a BB+PL and a 2BB after the outburst, as it approaches quiescence (Zhou et al. 2008). In the observation closest to quiescence, Zhou et al. find that $T_{\text{BB}} = 0.4$ keV in the BB+PL fit, and $T_{\text{BB}} = 0.37$ keV for the cooler component in the 2BB fit. Within these observational uncertainties, and accounting for the temperature corrections due to a magnetized Hydrogen atmosphere, our theoretically predicted temperature would be roughly consistent with the BB temperature measured for this object in quiescence.

Further constraints on our predictions for the thermal variables can be made through a comparison with the pulse profile and pulsed fraction of 1E 2259+586. We used the predicted temperature distribution to compute the expected flux from the pulsar during its rotation, and hence calculate the pulse profile and the pulsed fractions in selected energy bands. For this calculation, we included the general relativistic effects of gravitational redshift and light deflection, following the formalism of Page (1995), with the modifications by Perna & Gotthelf (2008). These allowed for the presence of a local anisotropic radiation pattern, $f(\delta) \propto \cos \delta^n$ (δ angle between the normal to the surface and the outgoing photon direction, and n a ‘beaming’ parameter, the only free parameter that we used to find a match to the observed level of modulation), as suggested by realistic atmospheric models. Realistic models were limited to fields perpendicular to the star surface, (e.g. van Adelsberg & Lai, 2006), and hence not directly applicable to the spectrum from the entire NS surface. However, we still use them to gauge the extent of the radiation beaming. Using the models of Van Adelsberg & Lai (2006), we find that, for $B \sim 10^{14}$ G and $T \sim 0.4$ keV, the intensity for $E \sim 1$ keV drops as $f(\delta) \propto \cos^2 \delta$ up to $\delta \lesssim 50$ deg and is shallower at larger δ ’s. The effect of absorption to the source (parameterized by the column density N_H) was also included in our calculations, since it has been shown to be important for the computation of the PF in finite energy bands (Perna et al. 2000).

We found the pulse profile to be double peaked, consistent with observations (Woods et al. 2004). We note that, for an orthogonal rotator (and more generally for a large angle between the line of sight and the rotation axis), the ‘‘double peaked’’ nature of the pulse profile is a very robust prediction of our temperature profile, since it is symmetric with respect to the equator. For $n = 1.5$, the pulsed fractions produced by the temperature profile of our simulations are 0.17 in the 0.3-1 keV band, and 0.22 in the 1-2 keV band. These values comfortably sit within the measured quiescent values for this source. However, we need to note that, given the BB plus powerlaw spectrum of this object, for the lowest energy band to be dominated by the thermal component, the powerlaw needs to have a cutoff in the soft X-ray band. This might be the case if hard

photons are due to upscattering of the thermal ones. We did not attempt to model the pulse profile in a quantitative fashion, given the substantial contamination from the non-thermal component, for which no predictions of its local angular distribution exist. A full spectral and timing analysis of the quiescent spectrum (as in Perna & Gotthelf 2008 and Gotthelf et al. 2010) is beyond the scope of this paper, and could only be performed with a better handle of the physical origin of the powerlaw.

PSR J1814-1744.

This object has a measured period $P = 3.975$ s and period derivative $\dot{P} = 7.4 \times 10^{-13}$ s/s (Camilo et al. 2000), yielding a timing age of 85 kyr. The dashed lines in Fig. 4 show the evolution of a similar object. The initial magnetic field set up in this case is $B_p = 1.6 \times 10^{14}$ G and $B_{\text{tor}} = 8 \times 10^{14}$ G. At the measured spin-down age of 85 kyr, the real age of the object is 60 kyr, with a predicted luminosity of about 4×10^{33} erg/s, 5 times smaller than in the previous case. At the same age, its period is 4.4 s, its spin-down rate 8×10^{-13} s/s, and its B_p about 9×10^{13} G. This is again in good qualitative agreement with the general properties of the object. Note that, for the X-ray luminosity, only upper limits exist. An analysis of *ROSAT* and *ASCA* archival data by Pivovarov et al. (2000) yielded the values $L_{0.1-2.4\text{keV}} < 6.3 \times 10^{35} d/10 \text{ kpc erg s}^{-1}$ from *ROSAT* and $L_{2-10\text{keV}} < 4.3 \times 10^{33} d/10 \text{ kpc erg s}^{-1}$ from the *ASCA* band. Our predicted thermal (bolometric) luminosity is consistent with these limits. Given the lack of X-ray detection, no comparison can be made at this stage with the pulse profile.

With these results, we have answered one of the puzzles: despite the second object under study has a similar dipolar field and is younger than the first example, its luminosity is substantially lower. Indeed, at other stages of evolution it can be even one order of magnitude smaller. The main reason for this difference, as we have discussed, is the larger initial toroidal field of the first example.

Now we face the next problem: can the two objects have a markedly different behaviour in their outbursting properties? To answer this question we have performed two simulations as described in Sect. 3, following the evolution of the two objects for another 10^4 yr but now using the code including the Hall term in the induction equation. For the same period of time, we found that the first object undergoes 753 starquakes, while the second one only had 23 of these events. On average, one would expect that the first kind of source shows an outburst every 10-20 years, while the second object only displays a magnetar-like activity every 4-5 centuries. Our results are summarized in Fig. 5. In addition to the much lower event rate, outbursts of objects like PSR J1814-1744 are also less energetic than the average magnetar outburst, thus making them harder to be observed. Therefore, the apparent dichotomy of the two objects with similar timing properties can easily be attributed to the slightly different initial poloidal field and, more importantly, to the much stronger internal toroidal field of one of the NSs.

5. SUMMARY

In this work we have performed a comprehensive study of starquake statistics on the NS crust, using the formalism developed by Perna & Pons (2011) for the coupled evolution of magnetic field and crust stresses during the lifetime of the NS. In particular, focusing on objects at age $10^4 - 10^5$ yr, we have

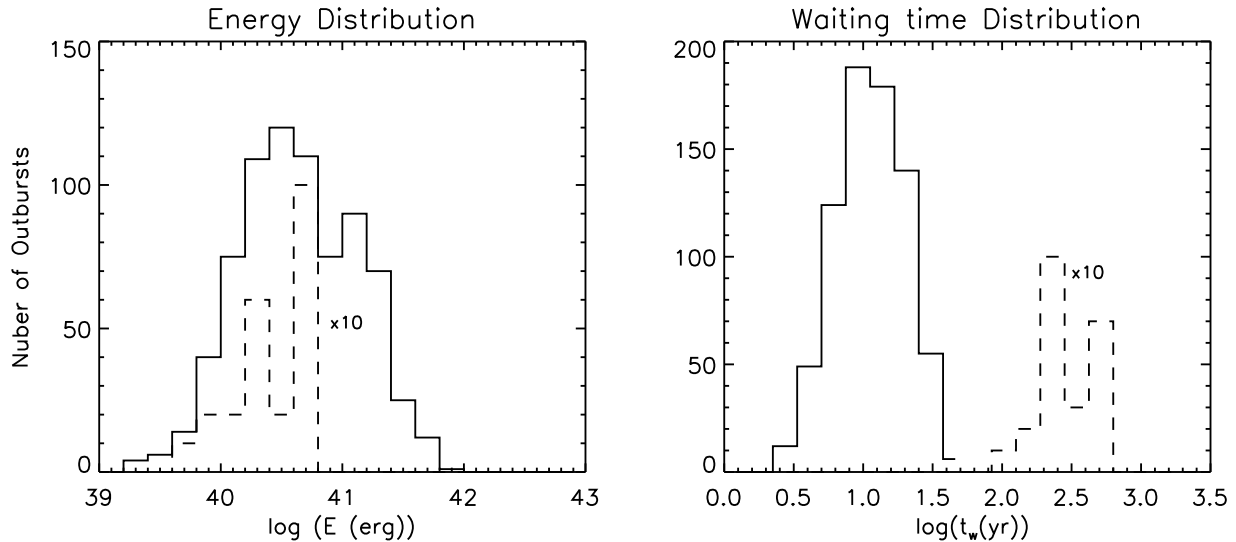


FIG. 5.— Energy and waiting time distribution of the two cases representative of 1E 2259+586 (solid) and PSR J1814-1744 (dashes). The latter case is magnified a factor of 10 for comparison. The total number of outbursts corresponds to a period of ten thousand years.

explored the dependence of the outburst frequency and energetics on the initial strengths of the dipolar and toroidal fields. We have found that the outburst frequency is negligible for initial poloidal fields below 10^{14} G, even when the initial toroidal field is extremely strong, $> 10^{16}$ G. The rate of outbursts is an increasing function of B_p (at fixed B_{tor}), and becomes significant (more than one per century) for $B_p(t=0) \gtrsim 5 \times 10^{14}$ G. On the other hand, at fixed B_p , the initial toroidal field has practically no influence on the starquake frequency for initial toroidal fields $B_{\text{tor}} \lesssim B_p$. This is because a toroidal field of the same order of magnitude of B_p is anyway rapidly formed on a Hall timescale. For initial $B_{\text{tor}} \gtrsim B_p$, the presence of the toroidal component affects the outburst rate, producing its rapid increase for initial B_{tor} much stronger than B_p .

The relative strengths of B_p and B_{tor} at birth also influence the thermal quiescent luminosity of the NS in a similar fashion. For negligible B_{tor} , the luminosity has a strong dependence on $B_p(t=0)$; it is about one order of magnitude larger for $B_p \sim 10^{15}$ G than it is for $B_p \sim 10^{13}$ G. The influence of the toroidal field becomes important, as for the outburst frequency, only for $B_{\text{tor}}(t=0) \gtrsim B_p(t=0)$.

>From our simulations, we can conclude that there is a critical value of the initial dipolar field strength, $B_p(t=0) \sim 3-5 \times 10^{14}$ G, above which some regular active periods may be expected. In this case, the intensity of the toroidal field at NS birth plays a crucial role in the ‘astrophysical appearance’ of those objects in their middle age. In fact, at around 10^5 yr, when B_p has roughly halved in strength to become $\sim 6-7 \times 10^{13}$ G, objects with negligible $B_{\text{tor}}(t=0)$ have an outburst rate below 1 per century, making them appear more like a quiet ‘high- B pulsar’. On the other hand, with a larger toroidal field at birth, an object with similar B_p can have an outburst rate of a few years, making it appear as a ‘magnetar’.

Correspondingly, due to the larger toroidal field, the thermal luminosity of the ‘magnetar’ is higher than that of the ‘high- B pulsar’. Interestingly, observations have shown that middle-aged objects with measured $B_p \sim 6-7 \times 10^{13}$ G can display radically different thermal and bursting properties. Specific examples are 1E 2259+586 and PSR J1814-1744: while they both have $B_p \sim 6 \times 10^{13}$ G, the former manifests itself as a magnetar, while the latter as a ‘high- B pulsar’. Here we have shown how appropriate choices of $B_p(t=0)$ and $B_{\text{tor}}(t=0)$ can naturally account for these differences, which no longer constitute a puzzle within the NS phenomenology.

The apparent dichotomy between *quiet*, high B-field radio-pulsars and *active* magnetars is not real. There is a continuum of possibilities, and all types of sources can potentially show some unusual activity (e.g. the recent case of SGR 0418+5729, Rea et al. 2010). We tend to classify them in classes according to a biased version of the anthropic principle: if it has several active periods on a human lifetime, we name it a magnetar; if it does not show an outburst on the same timescale, we put it in the group of quiet, normal neutron stars. But this separation is not necessarily associated to fundamental differences in the nature of the sources or their internal physics.

We thank an anonymous referee and Nanda Rea for helpful comments and suggestions. This work was partly supported by CompStar, a Research Networking Programme of the European Science Foundation and grants AYA2010-21097-C03-02, GVPROMETE02009-103 (JP) and NSF AST-1009396, NASA NNX10AK78G, NNX09AT17G, NNX09AT22G, NNX09AU34G, GO0-11077X, DD1-12052X, G09-0156X, AR1-12003X, DD1-12053X (RP).

REFERENCES

- Aguilera, D.N., Pons, J.A., & Miralles, J.A. 2008, A&A, 486, 255
 Arras, P., Cumming, A., & Thompson, C. 2004, ApJ, 608, L49
 Camilo, F., et al. 2000, ApJ, 541, 367
 Gavriil, F.P. & Kaspi, V. M. 2002, ApJ, 567, 1067
 Glampedakis, K., Jones, D.I., & Samuelsson, L. 2011, MNRAS, 413, 2021
 Gotthelf, E. V., Perna, R. & Halpern, J. P. 2010, ApJ, 724, 1316
 Kaspi, V. M., Gavriil, F. P., Woods, P. M., Jensen, J. B., Roberts, M. S. E., Chakrabarty, D. 2003, ApJ, 588L, 93
 Lloyd, D. 2003, PhD Thesis, Harvard University, Source DAI-B 64/05, p. 2228

- Page, D. 1995, *ApJ*, 442, 273
- Page, D., Prakash, M., Lattimer, J. M., & Steiner, A. W. 2011, *Phys. Rev. Lett.*, 106, 081101
- Page, D., Geppert, U., & Küker, M. 2007, *Ap&SS*, 308, 403
- Page, D., Lattimer, J. M., Prakash, M., & Steiner, A. W. 2004, *ApJS*, 155, 623
- Pérez-Azorín, J.F., Miralles, J.A., & Pons, J.A., 2006, *A&A*, 451, 1009
- Perna, R., Heyl, J., Hernquist, L. 2000, *ApJ*, 538L, 159
- Perna, R. & Gotthelf, A. V. 2008, *ApJ*, 681, 522
- Perna, R., & Pons, J.A. 2011, *ApJ*, 727, L51
- Pons, J.A., & Geppert, U. 2007, *A&A*, 470, 303
- Pons, J.A., Miralles, J.A., & Geppert, U. 2009, *A&A*, 496, 207
- Pivovarov, M. J., Kaspi, V. M., Camilo, F. 2000, *ApJ*, 535, 379
- Rea, N., et al. 2010, *Science*, 330, 944
- Shternin, P.S.; Yakovlev, D.G.; Heinke, C.O.; Ho, W.C.G. & Patnaude, D.J. 2011, *MNRAS*, 412, L108
- Suleimanov, V., Poutanen, J. Werner, K. 2011, *A&A*, 527, 139
- Tian, W. W., Leahy, D. A., Li, D. 2010, *MNRAS*, 404L, 1
- Thompson, C. & Duncan, R. C. 1995, *MNRAS*, 275, 255
- Thompson, C. & Duncan, R. C. 2001, *ApJ*, 561, 980
- van Adelsberg, M. & Lai, D. 2006, *MNRAS*, 373, 1495
- Woods, P. M., et al. 2004, *ApJ*, 605, 378
- Zhu, W., Kaspi, V. M., Dib, R., Woods, P. M., Gavriil, F. P., Archibald, A. M. 2008, *ApJ*, 686, 520